RSC Advances

PAPER

View Article Online
View Journal | View Issue

Cite this: *RSC Adv.*, 2019, **9**, 17783

Plasmonic nanoprobes based on the shape transition of Au/Ag core–shell nanorods to dumbbells for sensitive Hg-ion detection

Ling Chen,* Rui Li and Ping Yang *

We report a sensitive and selective localized surface plasmon resonance (LSPR) nanoprobe for the detection of mercuric ions (Hg^{2+}) using gold/silver core–shell nanorods as an optical nanosubstrate. Sulfide can quickly react with silver atoms to generate Ag_2S at room temperature in the presence of oxygen. The transformation from Ag shell to Ag_2S on the nanorod surface results in its LSPR absorption band shifting to a longer wavelength, which is attributed to their different refractive indices. Interestingly, the morphology also changed from a rod-like to dumbbell shape. However, in the presence of Hg^{2+}, this morphology transformation is inhibited because the sulfide reacts with free Hg^{2+} prior to the Ag atoms. The amount of Ag_2S reduced with the increasing concentration of Hg^{2+}, and the absorption band shift was also decreased. According to this "rod-like to dumbbell or not" shape change, a sensitive and selective LSPR nanoprobe was established, assisted by UV-Vis absorption spectroscopy. The detection limit of this probe for Hg^{2+} was as low as 13 nM. The efficiency of this probe in complex samples was evaluated by the detection of Hg^{2+} in spiked water samples.

Received 20th March 2019
Accepted 20th May 2019

DOI: 10.1039/c9ra02168j

rsc.li/rsc-advances

Introduction

Water pollution arising from toxic heavy metal ions has become a serious threat to human health and the ecological environment.[1,2] Heavy metal ions mainly exist in polluted water, with some also occurring in the atmosphere and solid waste. Heavy metals cannot be biodegraded, but they are bioaccumulative and can thus directly threaten higher organisms, including humans. Among these heavy metal ions, toxic mercury(II) ions in the form of organic or inorganic species are considered as a particularly harmful pollutant to human health, and such species are mainly distributed in water due to their water solubility[3,4] and can be enriched in the environment and in organisms causing damage to the brain, heart, kidneys, lungs, and immune system.[5] Therefore, the recognition and detection of mercury ions (Hg^{2+}) cannot be ignored. Current traditional analysis techniques for Hg^{2+} detection include atomic absorption spectroscopy, atomic emission spectroscopy, atomic fluorescence spectroscopy and inductively coupled plasma mass spectroscopy,[6–9] and these element-specific detection techniques are generally coupled with other accurate but sophisticated techniques, such as gas chromatography, high performance liquid chromatography and capillary electrophoresis.[10] Although these methods can provide good detection sensitivity, most of them require complex and sophisticated instruments and complicated operation procedures, which are time-consuming and laborious. Therefore, it is necessary to develop a simple, fast and low-cost method for the analysis of mercury ions.

Noble metallic nanoparticles with excellent localized surface plasmon resonance (LSPR) properties play a central role in optical nanoprobes for chemical and biological analysis.[11–14] Typically, plasmonic nanoparticle-based optical nanoprobes, such as colorimetric surface-enhanced Raman resonance probes, have been well developed for the detection and imaging of ions, small molecules, proteins, and cells.[15,16] In particular, colorimetric nanoprobes based on nanomaterials have attracted much attention due to their simplicity, rapidity and naked-eye detection.[17–19] In recent years, a series of optical nanoprobes for Hg^{2+} sensing have been developed based on plasmonic nanomaterials.[20–25] Most of these methods are based on noble metallic (gold or silver) nanomaterials with excellent optical properties. Specific recognition ligands, such as DNA aptamers, fluorescent molecules and small organic molecules, were employed for the specific recognition and detection of Hg^{2+} by using a colorimetric method assisted by absorption spectroscopy. For example, Yang's team developed a nano-sensing method that could be used to visualize and fluorescently respond to Hg^{2+} by using the principle that Hg^{2+} can induce configurational changes in thymine base-rich DNA and different electrostatic binding forces between single-stranded DNA/double-stranded DNA and gold nanoparticles.[26] Based on the strong affinity between gold and mercury, Campiglia *et al.* developed a colorimetric method based on the morphological changes of gold nanorods that could directly detect Hg^{2+} with

School of Materials Science and Engineering, University of Jinan, Jinan 250022, China. E-mail: mse_chenl@ujn.edu.cn; mse_yangp@ujn.edu.cn

quite low detection limit.[27] From the perspective of methodological research, these novel plasmonic nanoprobes show the application of gold or silver nanoparticles incisively and vividly, and also provide a new strategy for the detection of Hg^{2+}.

As a typical anisotropic nanoparticle, nanorods have two dimensions of width and length; their dipole plasmon resonance is split between transverse and longitudinal dipole resonances,[28] showing two absorption peaks in the spectrum. The position of the transverse and longitudinal absorption peaks depend on both the aspect ratio of the nanorods and the absolute dimensions of the particles. Different components of nanoparticles can also cause changes in the LSPR frequency as well as changes in the colloid's colour.[29,30] As for metal–metal core–shell nanoparticles, the plasmon resonance of the outer shell dominates; for instance, a blue-shift would strongly occur at the resonance of the Au/Ag core–shell particles.[31–33] As in a previous investigation, silver nanorods are more difficult to make than gold nanorods.[34] In this case, easily prepared-gold nanorods could be employed as the core section and their surface could be covered with a silver layer to fabricate pseudo-silver nanorods, which would also show the characteristic absorption peak of silver. This strategy offers a good candidate for diverse plasmonic nanoprobes.

In view of this characteristic, we initially prepared gold/silver core–shell composite nanorods and then established a suspension-based nanoprobe for the sensitive detection of mercury ions. Sulfide can quickly react with silver atoms to generate Ag_2S at room temperature in the presence of oxygen. The transformation from Ag shell to Ag_2S on the nanorod surface results in its LSPR absorption band shifting to a longer wavelength, attributed to their different refractive indices. However, in the presence of mercury ions, this morphology transformation would be inhibited because the sulfides react with free Hg^{2+} prior to Ag atoms. Thus, the sensing system for the detection of mercury ions was based on the different reaction abilities among sulfide anions, the silver shell and mercury ions.

Experimental section

Materials and methods

Hydrogen tetrachloroaurate(III) tetrahydrate ($HAuCl_4 \cdot 4H_2O$), sodium borohydride ($NaBH_4$), cetyltrimethylammonium bromide (CTAB), $AgNO_3$, ascorbic acid (AA), hydrochloric acid and sodium hydroxide were received from Sinopharm Chemical Reagent Co., Ltd, China. Sodium sulfide, $CoCl_2 \cdot 6H_2O$, $Cd(NO_3)_2$, $Pb(NO_3)_2$, $CuSO_4$, $Zn(NO_3)_2$, $MgSO_4$ and so on were purchased from Aladdin. The standard of $Hg(NO_3)_2$ (1000 ng mL^{-1}) was obtained from the CRM/RM Information Center of China. Because sodium sulfide is deliquescent, desiccative sodium sulfide was employed to prepare the sulfide solution. 0.12 g $Na_2S \cdot 9H_2O$ was weighed and dissolved in water in a 50 mL volumetric flask. The final concentration of sulfide was 0.01 mol L^{-1}. All the standards and stock solutions were stored at 4 °C in a refrigerator until further use. All of the chemicals and reagents were of analytical grade and used without further purification, and deionized ultrapure water was used for the preparation of the aqueous solutions in all of the experiments.

Deionized water (18.2 MΩ cm specific resistances) was purified by a Cascada TM LS Ultrapure water system (Pall Corp., USA). UV-Vis-NIR absorption spectra were measured on a HITACHI U-4100 spectrophotometer (Japan). The morphology of the synthesized samples was analyzed by transmission electron microscopy (TEM, JEM-2100, JEOL, Ltd, Japan). For sample preparation, the sediments were dropped on a copper mesh and dried in an oven at room temperature for observation by the transmission electron microscope. All the glasswares used in the following procedures was cleaned in a bath of freshly prepared aqua regia (HCl/HNO_3, 3v : 1v), rinsed thoroughly in water and dried in air.

Preparation of Au/Ag core–shell nanoparticles

Gold nanorods (Au NRs) were initially prepared *via* the most common method, namely "seed-mediated" growth as per a previous report[35] with some necessary modifications. Typically, for the seed solution, a freshly prepared, ice-cold aqueous $NaBH_4$ solution (0.01 M, 0.6 mL) was injected into a mixture solution of $HAuCl_4$ (0.05 M, 50 μL) and CTAB (0.1 M, 10 mL) under stirring at 28 °C. The resultant solution was stirred for 1 min and then kept at room temperature for 2 h. For the growth solution, $HAuCl_4$ (0.05 M, 0.4 mL), $AgNO_3$ (0.01 M, 0.4 mL) and CTAB (0.1 M, 40 mL) were mixed together, and then, a freshly prepared ascorbic acid solution (0.1 M, 0.32 mL) and an aqueous HCl solution (1.0 M, 0.8 mL) were added. After the resultant solution was mixed by stirring, the seed solution (100 μL) was rapidly injected with continuous stirring for 30 s. The reaction mixture was then left undisturbed overnight, with the temperature maintained at 26 °C.

For the growth of the silver shell, 4.0 mL of the as-synthesized Au NRs were purified by centrifugation for 20 min at 12 000 rpm, and re-dispersed with deionized water in the same volume. Then, 2.0 mL CTAB (0.1 M) was added to the Au NR solution with vigorous stirring. Afterwards, 300 μL 0.1 M AA and 400 μL 10 mM $AgNO_3$ were added to the mixture, followed by 600 μL 0.1 M NaOH to start the coating reaction within a few minutes. This reaction continued for 6 h. The resultant nanoparticles were then stored in glass media bottles and sealed at 4 °C in a refrigerator for the following experiments. The core–shell nanoparticles were washed by centrifugation before use in the sensing system.

Procedure for the sensing of mercury ions (Hg^{2+}) in aqueous solution

For Hg^{2+} sensing, the different concentrations of Hg^{2+} were first mixed with sulfide ions (2 μL, 0.01 M) in 0.5 mL buffer solution, and then the Au/Ag core–shell NRs (100 μL) were added. The total volume of the mixture was 1.5 mL. After incubation for several minutes, the absorption spectra were measured by using a UV-Vis spectrophotometer.

In the selectivity experiments, other metal ions (Co^{2+}, Cd^{2+}, Pb^{2+}, Cu^{2+}, Zn^{2+}, Ni^{2+}, Mg^{2+}) were tested in a similar way.

Analysis of mercury ions in real water samples

Drinking water and tap water samples obtained from our institute were filtered through a 0.2 μm membrane. The water

samples were spiked with standard Hg^{2+} ions at certain concentrations and then mixed with the stock solutions containing the Au/Ag core–shell NRs probe and an acetic acid–sodium acetate (HAc–NaAc) buffer solution (pH 5.0).

Results and discussion

Proposed mechanism of the Au/Ag nanorod-based plasmonic sensor for Hg^{2+} detection

Scheme 1 represents the proposed mechanism of the Au/Ag core–shell nanoparticle-based colorimetric assay for the detection of Hg^{2+} in an aqueous solution. The fabrication procedure of silver nanorods was much more difficult than that of gold nanorods. Therefore, the Au/Ag core–shell nanorods were designed by embedding a silver shell on the gold nanorods core section, whereby a blue-shift was expected and the resultant hybrid nanorods also possessed excellent LSPR properties. As shown in Fig. 1, the dominant absorption peak of the synthesized Au/Ag nanoparticles was around 630 nm, indicating the resonance of the outer silver shell, which also resulted in a deep green colour of the resultant colloid. Fig. 1B shows the rod-like shape of Au/Ag NRs having a 60 × 20 nm Au NR core and 2.5 nm Ag shell approximately. Interestingly, the resultant hybrid nanoparticle revealed that an anisotropic coating of silver occurred, resulting in partly orange slice-like nanocrystals. Different growth rates for the {110} side facets accounted for this shape.[36] Among the four {110} side facets, two of the neighbouring {110} facets grew quickly and another two grew comparatively slowly, thus inducing the anisotropic deposition of the silver shell.

In the presence of oxygen, sulfide ions can selectively and quickly react with silver atoms to generate Ag_2S at room temperature,[37,38] under basic conditions:

$$4Ag + 2S^{2-} + O_2 + 2H_2O \rightarrow 2Ag_2S + 4OH^-$$

and under acidic conditions:

$$4Ag + 2S^{2-} + O_2 + 4H^+ \rightarrow 2Ag_2S + 2H_2O$$

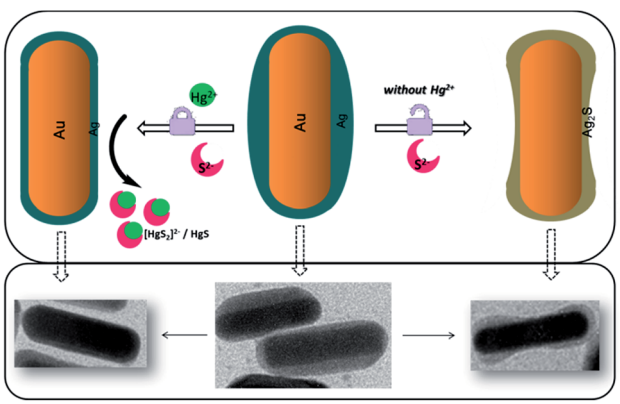

Scheme 1 Au/Ag core–shell nanoparticle-based sensing method for the detection of Hg^{2+}.

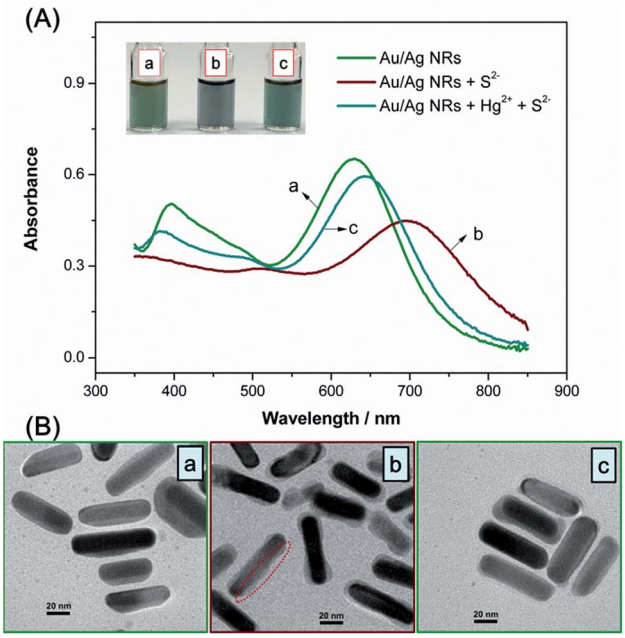

Fig. 1 (A) UV-Vis absorbance spectra of Au/Ag core–shell nanorods at different conditions: (a) Au/Ag core–shell NRs; (b) Au/Ag core–shell NRs + S^{2-} (10 μM) (c) Au/Ag core–shell NRs + Hg^{2+} (3 μM) + S^{2-} (10 μM). Inset image shows the corresponding colloid colour. (B) TEM images of nanoparticles corresponding to different conditions in (A).

In this case, the formation of Ag_2S on an Au/Ag core–shell nanoparticle surface would result in its LSPR maximum shifting to a longer wavelength because the refractive indices of Ag (~0.17) and Ag_2S (~2.2) are substantially different. As shown in Fig. 1A, curves (a) and (b), the absorption peak shifted from 630 nm to 700 nm after the introduction of sulfide anions. The colloid colour also changed from blue-green to blue-grey.

According to Fig. 1B(b), the TEM image of Au/Ag NRs with a certain amount of S^{2-} indicated that the resultant shell was irregular. Meanwhile, interestingly, after the reaction with sufficient sulfide ions, the morphology of the nanoparticles was transformed from rod-like to dumbbell shaped, according to the SEM images in Fig. 2. We assume that this transformation was mainly attributed to the following reasons. The volume of one Ag_2S unit is larger than that of two Ag atoms following the incorporation of S^{2-}.[39] During the sulfidation reaction, the new Ag_2S shell expands outward and forms irregular stacks at specific points. It is worth noting that Ag_2S gives priority to stacking at the endcap site with a small curvature radius,[38] and finally forms a dumbbell shape with sufficient sulfide ions. The high-resolution TEM image (Fig. 2c) confirmed the formation of the Ag_2S shell near the endcap sites with an interplane distance of the lattice fringes of ~0.28 nm, corresponding to that of the (−112) facets of Ag_2S.[40]

Then, wonderfully, mercury ions could "inhibit" this change due to the strong affinity between Hg and S. Herein, mercury ions could preferentially consume sulfides, resulting in decreased Ag_2S formation. It is also noted that the pK_{sp} of Ag_2S was 48.7, HgS was 52.4,[41] and according to the stoichiometric

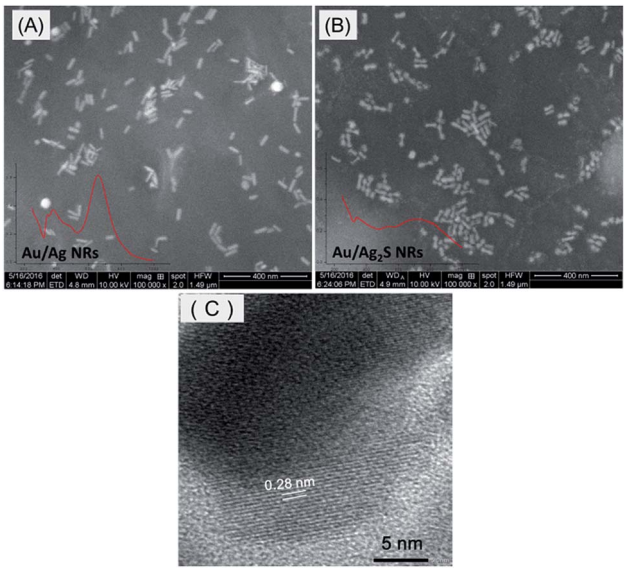

Fig. 2 SEM images of Au/Ag core–shell nanorods (A) and Au/Ag_2S nanoparticles (B). High-resolution TEM image of Au/Ag_2S nanoparticles (C).

ratio, log[Ag–S] was −16.23 and log[Hg–S] was −26.2, indicating the stronger affinity between Hg and S. As in a previous representative report, Hg^{2+} could bind with S^{2-} by forming HgS with the equivalent S^{2-} or $[HgS_2]^{2-}$ species with excess S^{2-}.[42] The obvious sensing of Hg^{2+} in this well-designed system was confidently expected.

As suggested by Fig. 1A, curve (c), while adding a moderate concentration of Hg^{2+}, the absorption peak was retained at 650 nm. The solution colour changes were in accordance with the absorption spectra change. According to the TEM images, after adding the sulfide, the Au/Ag core–shell nanorods were invaded and the shell morphology transformed to be an irregular partly dumbbell shape (Fig. 1B(b)), while in the presence of Hg^{2+}, the nanoparticles stayed in a rod-like shape (Fig. 1B(c)); in this case, sulfide prior reacted first with Hg^{2+} due to the strong interaction between S and Hg species. On the basis of this "rod-like to dumbbell or not" phenomenon, a sensing method for Hg^{2+} detection was established based on Au/Ag nanorods with the assistance of sulfide.

It is well known that the frequency of LSPR can be tuned by changing the material composition, size, shape and dielectric environment.[43] Other reports of mercury sensors based on nanorods or nanoparticles involved aggregation,[44] amalgamation,[45] etching[46,47] or other effects that can be modulated by mercury; hence, discussing these effects is necessary. The aggregation of nanoparticles indeed can lead to red-shifts and assembly *via* side by side or end to end. In the recent work by Zhu *et al.*, cysteine was modified on the surface of nanorods to mediate the assembly.[44] In this work, no ligands were introduced to induce the aggregating behaviour of nanoparticles. As indicated by the TEM images in Fig. 1B, the nanoparticles exhibited a well-monodispersed state. Besides, the colloid colour was transparent and no precipitate emerged after staying for a few days. Therefore, we can firmly state that the red-shift of the absorbance spectra could be attributed to the substantially different refractive indices of Ag (~0.17) and Ag_2S (~2.2).

Mercury is known to form amalgams with gold and silver. Jin and Han describe how the formation of such amalgams can alter the SPR of gold nanorods.[45] They use ascorbic acid as a reducing agent. Here, the Au/Ag core–shell nanorods were washed by centrifugation before using in the sensing system. The effect of the ascorbic acid involved in the synthesis procedure was negligible. Ying Qi *et al.* developed a typical determination strategy for Hg^{2+} based on the surface etching of Au–Ag core–shell triangular nanoplates.[47] It is reported that the formation of a chemical complex will reduce the activity of ions and therefore reduce the redox potential.[48,49] In this work, it is worth noting that Hg^{2+} was mixed with sulfide first, and then the Au/Ag core–shell nanorods were added. In this case, HgS or HgS_2^{2-} should be considered instead of bare Hg^{2+}. According to the Nernst equation, $E = E_0 + \frac{RT}{nF} \ln \frac{[Ox]}{[Red]}$, due to the formation of HgS or HgS_2^{2-}, the potential will be substantially decreased. Thus the potential energy barrier between Hg^{2+} and Ag is increased. According to the TEM images, the etching by Hg^{2+} was difficult to observe.

Optimal sensing conditions of the proposed plasmonic nanoprobe

To obtain the best performance for the sensing system, the sensing conditions were examined in detail, such as pH condition, concentration of sulfide, the effects of other anions and the reaction time. The LSPR maximum shift, $\Delta\lambda_{max}$ value, was employed to evaluate the absorption peak shift.

According to the respective reaction of Ag and Hg with sulfide ions, acidic condition is beneficial to the reaction system.[50] Thus, to avoid the H_2S gas escaping in acidic condition with low pH, and promote the reaction between Ag or Hg with S, acid buffer solutions with a relatively higher pH were introduced into the sensing system. As can be seen in Fig. 3 A, the proposed sensing system was not quite sensitive to pH 4.2–6.0. Accordingly, HAc–NaAc buffer solution (pH ~5.0) was chosen for further experiments.

Under acidic conditions, H_2S will be the major species. This also could be confirmed by calculating the distribution fractions of the existing sulfide species. H_2S is a typical diacid; the two dissociation constants are $K_{a_1} = 1.3 \times 10^{-7}$, $K_{a_2} = 7.1 \times 10^{-15}$, and[41] δ_2, δ_1, δ_0 represent the distribution fraction of H_2S, HS^-, S^{2-}, respectively. In theory,

$$\delta_2 = \frac{[H_2S]}{[H_2S] + [HS^-] + [S^{2-}]} = \frac{1}{1 + \frac{[HS^-]}{[H_2S]} + \frac{[S^{2-}]}{[H_2S]}}$$

$$= \frac{1}{1 + \frac{K_{a_1}}{[H^+]} + \frac{K_{a_1}K_{a_2}}{[H^+]^2}} = \frac{[H^+]^2}{[H^+]^2 + K_{a_1}[H^+] + K_{a_1}K_{a_2}}$$

$$\delta_1 = \frac{[HS^-]}{[H_2S] + [HS^-] + [S^{2-}]} = \frac{K_{a_1}[H^+]}{[H^+]^2 + K_{a_1}[H^+] + K_{a_1}K_{a_2}}$$

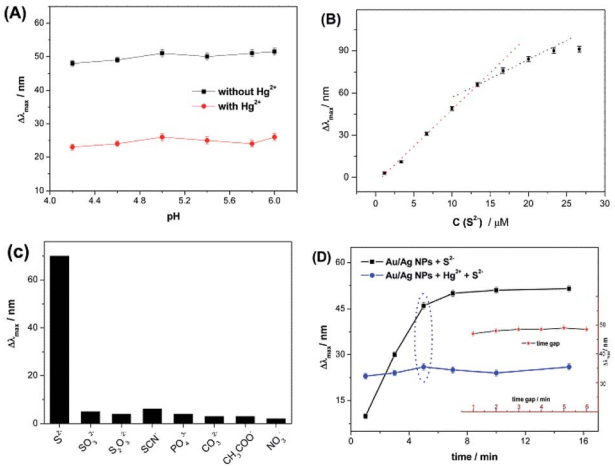

Fig. 3 Optimization of the sensing conditions: (A) effect of pH; (B) effect of the concentration of sulfide in the sensing system; (C) effects of other anions. (D) Effect of reaction time, inset: effect of time gap. Error bars represent the standard deviations based on three independent measurements.

$$\delta_0 = \frac{[S^{2-}]}{[H_2S] + [HS^-] + [S^{2-}]} = \frac{K_{a_1}K_{a_2}}{[H^+]^2 + K_{a_1}[H^+] + K_{a_1}K_{a_2}}$$

According to the above formulas, the values of δ_2, δ_1, δ_0 can be calculated, where, $\delta_2 = 0.9872$, which means H_2S will be the major species.

In the practical sensing system, four reactions are involved as below.

$$H_2S \rightleftharpoons H^+ + HS^- \quad (1)$$

$$HS^- \rightleftharpoons H^+ + S^{2-} \quad (2)$$

$$4Ag + 2S^{2-} + O_2 + 4H^+ \rightarrow 2Ag_2S + 2H_2O \quad (3)$$

$$Hg^{2+} + S^{2-} \rightarrow HgS \quad (4)$$

The latter two reactions (eqn (3) and (4)) are irreversible; the formation constant of Ag_2S and HgS are sufficiently high, and thus the two reversible reactions are driven to dissociation, promoting the sensing behaviour.

Sulfides can quickly react with silver atoms in the presence of oxygen by generating Ag_2S at room temperature. Because of the different refractive indices of Ag and Ag_2S, the formation of Ag_2S on the Au/Ag core–shell nanoparticle surface would result in its LSPR maximum shifting to a longer wavelength.[51] Increasing amounts of sulfide were added to the nanoparticles, whereby a red-shift of the LSPR absorption band occurred gradually. The $\Delta\lambda_{max}$ value was recorded to evaluate the absorption peak shift. Finally, 13.3 μM was chosen, at which the increasing trend of $\Delta\lambda_{max}$ value reached maximum, as shown in Fig. 3B. In this case, while adding Hg^{2+}, a remarkable absorption band change along this trend can be expected. The effects of inorganic sulfur ions ($S_2O_3^{2-}$, SO_3^{2-}, SCN^-) and other anions (NO_3^-, CH_3COO^-, PO_4^{3-}, CO_3^{2-}) on the sensing system were also examined. As indicated in Fig. 3C, no comparable LSPR responses from other species were detected because of the much lower solubility of Ag_2S ($pK_{sp} = 50.83$) than other Ag compounds.

As the reaction proceeds, the absorbance spectra of the nanoparticles changed gradually. Thus, the spectra were recorded continuously to indicate the reaction extent. The reaction time was also studied under the optimized pH in the absence and presence of Hg^{2+}. The results showed that the maximum band shift was obtained in 5 min after the addition of Hg^{2+} and remained unchanged with further increases in reaction time. Additionally, the time gap between the additions of nanorods after sulfide interaction was also tested. It was found that the effects of different time gaps could be negligible (inset of Fig. 3D).

Feasibility for the detection of Hg^{2+}

To quantify the concentration of Hg^{2+}, $R\ (\%) = (\lambda_S - \lambda_{Hg})/(\lambda_S - \lambda_{blank})$, this ratio value was employed to indicate the extent of inhibition by Hg^{2+} against the sulfide, where λ_S, λ_{Hg}, and λ_{blank} represent the LSPR absorbance band of Au/Ag nanorod colloid solution in three different conditions: in the presence of a certain amount of sulfide alone, sulfide and Hg^{2+}, absence of both, respectively. Fig. 4B shows a corresponding calibration

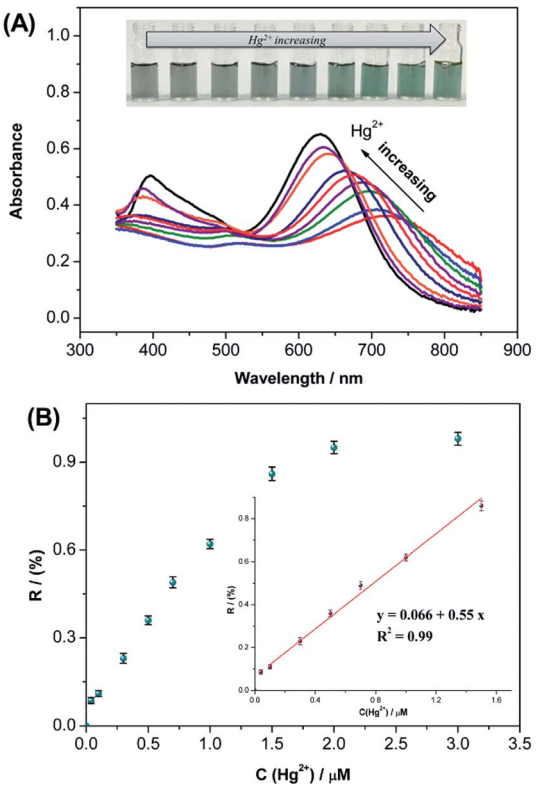

Fig. 4 (A) UV-Vis spectra of the Au/Ag core–shell NRs sensing system with different concentrations of Hg^{2+}; inset image shows the colorimetric response to different concentrations of Hg^{2+} (0, 0.04, 0.1, 0.3, 0.5, 0.7, 1.0, 1.5, 2.0, 3.0 μM, respectively). (B) The ratio of R (%) = $(\lambda_S - \lambda_{Hg})/(\lambda_S - \lambda_{blank})$ as a function of the different concentrations of Hg^{2+}, the inset shows a linear relationship from 0.04 to 1.5 μM. The incubation time was 5 min; the error bars represent the standard deviations based on three independently measured values.

Table 1 Comparison of plasmonic nanoparticle-based methods for the determination of Hg^{2+}

Optical techniques	Fabrication of sensors	Limit of detection (nM)	Linear range	References
Colorimetry/UV-Vis	3-Mercaptopropionate acid-Au NPs	100	0.2–0.5 μM	53
	Cysteine-AuNPs	25	0.05–1, 1–10 μM	54
	Peptite-AuNPs	20	10–45 μM	55
	Mercaptopropionate acid/AMP-Au NPs	500	0.5–3.5 μM	56
	Dithioerythritol-AuNPs	24	0.1–0.5, 0.5–5 μM	22
	Chitosan-$MoSe_2$ nanosheets with TMB	3.5	0.025–2.5 μM	57
Fluorescence	BAS/R6G/MPA-AuNPs	20	0.1–2.5 μM	58
UV-Vis	Au/Ag core–shell nanorods	13	0.04–1.5 μM	This work

plot of the ratio value R with the concentration of Hg^{2+} ranging from 0 to 3.0 μM. As shown by the inset of Fig. 4B, a good linear relationship was exhibited from 0.04 to 1.5 μM ($R^2 = 0.99$), and the limit of detection was estimated to be about 13 nM at a signal-to-noise ratio of 3. This value is particularly attractive because it is lower than the maximum level (30 nM) permitted by the World Health Organization (WHO).[52] Skillfully, the sensing range can be tuned by the amount of nanoparticles involved in the sensing behaviour, that is to say, more nanoparticles in the sensing system will expand the sensing range, and *vice versa*. Compared with other works, this proposed method does not need a ligand to functionalize the nanoparticle. According to the parameters given in Table 1, this work also exhibits competitive performance for mercury ion detection, including the detection limit and sensing range.

A specific response towards a target is of great significance for a nanoprobe. The excellent selectivity of this method for mercury ions over competing species can be expected by comparing the stability constant ($\log K_f$) of metallic ions with sulfide ions. We next examined the selectivity of the proposed sensing method by obtaining the absorbance spectra in the presence of other metal ions, such as Co^{2+}, Cd^{2+}, Pb^{2+}, Cu^{2+}, Zn^{2+}, Ni^{2+}, and Mg^{2+}. As shown in Fig. 5, among all the metal ions examined, only Hg^{2+} caused a significant response. Other metal ions could not bind with the S anions effectively, and their effects on the sensing behaviour were negligible. It is known that those metal ions (*e.g.* Cu^{2+}, Pb^{2+}, Zn^{2+}) can interact with sulfide ions to form respective metal sulfides. The difference in their formation constants was employed here. We note that the $\log K_f$ of Hg(ITC) n was *ca.* 21.8, whereas those of Cu^{2+}, Pb^{2+}, Zn^{2+} were 10.4, 1.48, 2.0,[59] respectively, indicating that Hg^{2+} has the higher affinity toward sulfide species. Under the optimal conditions, the absorption spectra were recorded and no obvious response was obtained with other metal ions. Therefore, the selective detection of Hg^{2+} stems indeed from the strong and selective interaction between Hg^{2+} and sulfide.

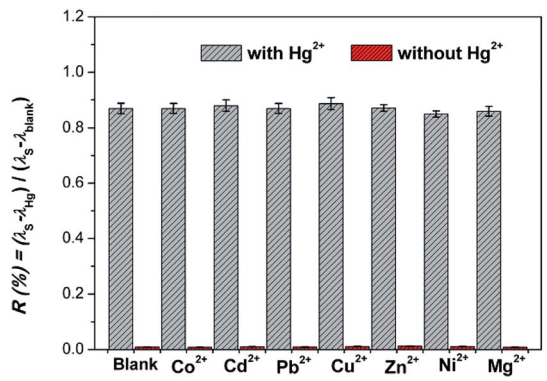

Fig. 5 The ratio of R (%) = $(\lambda_S - \lambda_{Hg})/(\lambda_S - \lambda_{blank})$ of an Au/Ag core–shell NR-based sensing system in the presence of 1.5 μM of Hg^{2+}, 10-fold other competing ions (15 μM) including Co^{2+}, Cd^{2+}, Pb^{2+}, Cu^{2+}, Zn^{2+}, Ni^{2+}, Mg^{2+}. Error bars represent the standard deviations based on three independent measurements.

Practical analysis of Hg^{2+} in water samples

The efficiency of the sensing performance of the established plasmonic nanoprobe was further investigated for its practical applicability towards Hg^{2+} analysis. Drinking water and tap water samples were collected and employed as a complicated matrix. No mercury ions were detected in the initial water samples. Different concentrations of mercury ions were introduced into the samples to simulate polluted water samples, and then the added Hg^{2+} was detected using our proposed nanoprobe. As shown in Table 2, satisfactory recoveries were obtained in the range of 96.7–102.7% for the two practical water samples, drinking water and tap water, with spiked concentration levels of Hg^{2+}. The results clearly confirmed that this proposed nanoprobe is potentially applicable for the accurate determination of mercury ions in real samples. In this Au/Ag core–shell nanorod-based sensing system, Hg^{2+} ions were detected indirectly assisted by sulfide ions. From the angle of methodology, we designed a method for Hg^{2+} sensing based on the shell morphology change of plasmonic nanoparticles. As for the

Table 2 Recoveries of the nanoprobe for the determination of mercury ions in drinking water and tap water samples ($n = 5$)[a]

Samples	Spiked (nM)	Found (nM)	Recovery (%)	RSD (%)
Drinking water	0	nd	—	—
	300	290.1	96.7	0.72
	600	612.5	102.1	1.13
	1000	968.5	96.85	1.05
Tap water	0	nd	—	—
	300	308.2	102.7	1.03
	600	615.5	102.6	1.24
	1000	998.7	99.87	1.45

[a] nd: not detected.

application in more complicated samples, which may themselves contain sulfide/sulfate ions, limitations exist objectively. Integrating the methodology and application, an additional job-plot could be established in real samples to avoid the presence of sulfide ions.

Conclusions

In conclusion, a sensitive and selective localized surface plasmon resonance (LSPR) nanoprobe for the detection of mercuric ions was fabricated by using gold/silver core–shell nanorods. Sulfides play an important role by quickly reacting with silver atoms to generate Ag_2S at room temperature in the presence of oxygen. The transformation from the silver shell to Ag_2S on the nanorod surface resulted in its LSPR absorption band shifting to a longer wavelength because of their different refractive indices. Interestingly, the morphology also changed from rod-like to dumbbell shaped. But, in the presence of mercury ions, this morphology transformation was inhibited because the sulfide could preferentially react with free Hg^{2+} instead of Ag atoms. The amount of Ag_2S was reduced with the increasing concentration of Hg^{2+}, and the absorption band shift also decreased. According to this "rod-like to dumbbell or not" shape change, a sensitive and selective LSPR nanoprobe was developed that was assisted by UV-Vis absorption spectroscopy. A good linear relationship was obtained between the absorption band shift and Hg^{2+} concentrations. The detection limit of this sensor towards Hg^{2+} was as low as 13 nM, which is lower than the limitation concentration (30 nM) proposed by the World Health Organization. The efficiency of this probe in complex samples was evaluated by allowing the detection of Hg^{2+} in spiked water samples. A satisfactory recovery was obtained, which indicates its promising potential for application in complicated environmental areas.

Conflicts of interest

There are no conflicts to declare.

Acknowledgements

This research was supported by the National Natural Science Foundation of China (51501071, 51572109 and 51772130), the Outstanding Young Scientists Foundation Grant of Shandong Province (BS2014CL037), General Grant Financial from China Postdoctoral Science Foundation (Grant No: 2016M592124).

References

1 A. Alsbaiee, B. J. Smith, L. Xiao, Y. Ling, D. E. Helbling and W. R. Dichtel, *Nature*, 2016, **529**, 190–194.
2 D. Banerjee, D. Kim, M. J. Schweiger, A. A. Kruger and P. K. Thallapally, *Chem. Soc. Rev.*, 2016, **45**, 2724–2739.
3 R. Das, C. D. Vecitis, A. Schulze, B. Cao, A. F. Ismail, X. Lu, J. Chen and S. Ramakrishna, *Chem. Soc. Rev.*, 2017, **46**, 6946–7020.
4 J. R. Miller, J. Rowland, P. J. Lechler, M. Desilets and L.-C. Hsu, *Water, Air, Soil Pollut.*, 1996, **86**, 373–388.
5 P. B. Tchounwou, W. K. Ayensu, N. Ninashvili and D. Sutton, *Environ. Toxicol.*, 2003, **18**, 149–175.
6 K. Leopold, M. Foulkes and P. Worsfold, *Anal. Chim. Acta*, 2010, **663**, 127–138.
7 S. R. Segadea and Ju. F. Tyson, *Talanta*, 2007, **71**, 1696–1702.
8 M. Leermakers, W. Baeyens, P. Quevauviller and M. Horvat, *Trends Anal. Chem.*, 2005, **24**(5), 383–393.
9 K. Leopold, M. Foulkes and P. J. Worsfold, *Trends Anal. Chem.*, 2005, **28**(4), 426–435.
10 F. F. Yang, J. H. Li, W. H. Lu, Y. Y. Wen, X. Q. Cai, J. M. You, J. P. Ma, Y. J. Ding and L. X. Chen, *Electrophoresis*, 2014, **35**, 474–481.
11 K. Saha, S. S. Agasti, C. Kim, X. Li and V. M. Rotello, *Chem. Rev.*, 2012, **112**, 2739–2779.
12 E. Boisselier and D. Astruc, *Chem. Soc. Rev.*, 2009, **38**, 1759–1782.
13 A. Kumar, S. Kim and J.-M. Nam, *J. Am. Chem. Soc.*, 2016, **138**, 14509–14525.
14 P. K Jain, X. H. Huang, I. H. EL-Sayed and M. A. EL-Sayed, *Acc. Chem. Res.*, 2008, **41**, 1578–1586.
15 L. X. Chen, Y. Q. Wang, X. L. Fu, L. Chen, *Novel Optical Nanoprobes for Chemical and Biological Analysis*, 2014, DOI: 10.1007/978-3-662-43624-0.
16 S. K. Kailasa, J. R. Koduru, M. L. Desai, T. J. Park, R. K. Singhal and H. Basu, *TrAC, Trends Anal. Chem.*, 2018, **105**, 106–120.
17 D. Liu, Z. Wang and X. Jiang, *Nanoscale*, 2011, **3**, 1421–1433.
18 V. N. Mehta and S. K. Kailasa, *RSC Adv.*, 2015, **5**, 4245–4255.
19 S. K. Kailasa, M. Chandel, V. N. Mehta and T. J. Park, *Spectrochim. Acta, Part A*, 2018, **195**, 120–127.
20 J. Du, L. Jiang, Q. Shao, X. Liu, R. S. Marks, J. Ma and X. D. Chen, *Small*, 2013, **9**, 1467–1481.
21 Y. Ding, S. Wang, J. Li and L. Chen, *Trends Anal. Chem.*, 2016, **82**, 175–190.
22 H. Zhang and Y. S. Xia, *ACS Sens.*, 2016, **1**, 384–391.
23 L. L. He, L. Cheng, Y. Lin, H. F. Cui, N. Hong, H. Peng, D.-R. Kong, C. –D. Chen, J. Zhang, G. B. Wei and H. Fan, *J. Electroanal. Chem.*, 2018, **814**, 161–167.
24 C. Zhang, C. Kong, Q. Liu and Z. Chen, *Analyst*, 2019, **144**, 1205–1209.
25 D. Huang, X. Liu, C. Lai, L. Qin, C. Zhang, H. Yi, G. Zeng, B. Li, R. Deng, S. Liu and Y. Zhang, *Microchim. Acta*, 2019, **186**, 31.
26 H. Wang, Y. Wang, J. Jin and R. Yang, *Anal. Chem.*, 2008, **80**, 9021–9028.
27 M. Rex, F. E. Hernandez and A. D. Campiglia, *Anal. Chem.*, 2006, **78**, 445–451.
28 S. Link and M. A. El-Sayed, *J. Phys. Chem. B*, 1999, **103**, 8410–8426.
29 J. Becker, I. Zins, A. Jakab, Y. Khalavka, O. Schubert and C. Sönnichsen, *Nano Lett.*, 2008, **8**, 1719–1723.
30 Y. Xiang, X. Wu, D. Liu, Z. Li, W. Chu, L. Feng, K. Zhang, W. Zhou and S. Xie, *Langmuir*, 2008, **24**, 3465–3470.
31 M. B. Cortie and A. M. McDonagh, *Chem. Rev.*, 2011, **111**, 3713–3735.

32 Y. Xiang, X. Wu, D. Liu, Z. Li, W. Chu, L. Feng, K. Zhang, W. Zhou and S. Xie, *Langmuir*, 2008, **24**, 3465–3470.
33 T. Kim, Q. Zhang, J. Li, L. Zhang and J. V. Jokerst, *ACS Nano*, 2018, **12**, 5615–5625.
34 D. Seo and H. Song, *J. Am. Chem. Soc.*, 2009, **131**, 18210–18211.
35 Y. D. Zheng, M. D. Xiao, S. X. Jiang, F. Ding and J. F. Wang, *Nanoscale*, 2013, **5**, 788–795.
36 Z. L. Wang, *J. Phys. Chem. B*, 2000, **104**, 1153–1175.
37 S. Lilienfeld and C. E. White, *J. Am. Chem. Soc.*, 1930, **52**, 885–892.
38 J. Zeng, J. Tao, D. Su, Y. Zhu, D. Qin and Y. Xia, *Nano Lett.*, 2011, **11**, 3010–3015.
39 G. Park, C. Lee, D. Seo and H. Song, *Langmuir*, 2012, **28**, 9003–9009.
40 Y. Du, B. Xu, T. Fu, M. Cai, F. Li, T. Zhang and Q. Wang, *J. Am. Chem. Soc.*, 2010, **132**, 1470–1471.
41 Wuhan University, *Analytical Chemistry, addenda, Solubility product of slightly soluble compounds*, 2008, pp. 402–403.
42 S. Y. Ding, M. Dong, Y. W. Wang, Y. T. Chen, H. Z. Wang, C. Y. Su and W. Wang, *J. Am. Chem. Soc.*, 2016, **138**, 3031–3037.
43 P. K. Jain, K. S. Lee, I. H. EI-Sayed and M. A. EI-Sayed, *J. Phys. Chem. B*, 2006, **110**, 7238–7248.
44 J. Zhu, B. Z. Zhao, Y. Qi, J. J. Li, X. Li and J. W. Zhao, *Sens. Actuators, B*, 2018, **255**, 2927–2935.
45 L. H. Jin and C. S. Han, *Sens. Actuators, B*, 2014, **195**, 239–245.
46 J. Zhu, T. T. Jia, J. J. Li and J. W. Zhao, *Spectrochim. Acta, Part A*, 2019, **207**, 337–347.
47 Y. Qi, J. Zhao, G. J. Weng, J. J. Li, J. Zhu and J. W. Zhao, *Sens. Actuators, B*, 2018, **267**, 181–190.
48 J. Rodríguez-Fernández, J. Pérez-Juste, P. Mulvaney and L. M. Liz-Marzán, *J. Phys. Chem. B*, 2005, **109**, 14257–14261.
49 L. Shang, L. H. Jin and S. J. Dong, *Chem. Commun.*, 2009, 3077–3079.
50 D. Liu, S. Wang, M. Swierczewska, X. Huang, A. A. Bhirde, J. Sun, Z. Wang, M. Yang, X. Jiang and X. Chen, *ACS Nano*, 2012, **6**(12), 10999–11008.
51 B. Xiong, R. Zhou, J. Hao, Y. Jia, Y. He and E. S. Yeung, *Nat. Commun.*, 2013, **4**, 1708, DOI: 10.1038/ncomms2722.
52 World Health Organization, *Guidelines for drinking-water quality: incorporating 1st and 2nd addenda, volume 1–Recommendations*, World Health Organization, Geneva, 3rd edn, 2008, http://www.who.int/water_sanitation_health/dwq/fulltext.pdf.
53 C. C. Huang and H. T. Chang, *Chem. Commun.*, 2007, **12**, 1215–1217.
54 N. Ding, H. Zhao, W. Peng, Y. He, Y. Zhou, L. Yuan and Y. Zhang, *Colloids Surf., A*, 2012, **395**, 161–167.
55 S. Si, A. Kotal and T. K. Mandal, *J. Phys. Chem. C*, 2007, **111**(3), 1248–1255.
56 C. J. Yu and W. L. Tseng, *Langmuir*, 2008, **24**(21), 12717–12722.
57 L. Huang, Q. Zhu, J. Zhu, L. Luo, S. Pu, W. Zhang, W. Zhu, J. Sun and J. Wang, *Inorg. Chem.*, 2019, **58**, 1638–1646.
58 H. Y. Chang, T. M. Hsiung, Y. F. Huang and C. C. Huang, *Environ. Sci. Technol.*, 2011, **45**(4), 1534–1539.
59 D. Liu, S. Wang, M. Swierczewska, X. Huang, A. A. Bhirde, J. Sun, Z. Wang, M. Yang, X. Jiang and X. Chen, *ACS Nano*, 2012, **6**(12), 10999–11008.